JACS
JOURNAL OF THE AMERICAN CHEMICAL SOCIETY
Article
pubs.acs.org/JACS

Mechanism of Cobalt Self-Exchange Electron Transfer

Andrew M. Ullman and Daniel G. Nocera*

Department of Chemistry and Chemical Biology, Harvard University, 12 Oxford Street, Cambridge, Massachusetts 02138, United States

Supporting Information

ABSTRACT: A heptanuclear cobalt cluster was synthesized in two different oxidation states, $Co(II)_7$ and a mixed valence $Co(III)Co(II)_6$, as a soluble model of a cobalt−phosphate/borate (Co-OEC) water splitting catalyst. Crystallographic characterization indicates similar cluster cores, distinguished primarily at the central Co atom. An anion associates to the cluster cores via hydrogen bonding. Using an isotope exchange method, an anomalously slow self-exchange electron transfer rate constant (k_{obs} = 1.53 × 10^{-3} M^{-1} s^{-1} at 40 °C and 38 mM [OTf] in MeCN), as compared to that predicted from semiclassical Marcus theory, supports a charge transfer process that is accelerated by dissociation of the anion from the oxidized cluster. This mechanism sheds light on the inverse dependence of anions in the self-repair mechanism of Co-OECs. Moreover, because H_2O cannot directly bridge cobalt centers, owing to the encapsulation of the central Co within the cluster core, the observed results address a long-standing controversy surrounding the $Co^{2+/3+}$ self-exchange electron transfer reaction of the hexaaqua complex.

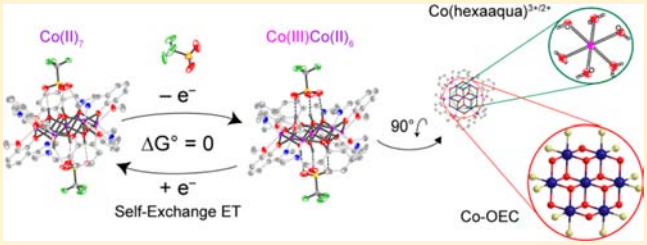

INTRODUCTION

Oxidation of Co^{2+} to Co^{3+} in the presence of phosphate (P_i), methyl phosphonate (MeP_i), or borate (B_i) results in the self-assembly of cobalt clusters that are active water-splitting catalysts.[1−4] The cobalt oxygen evolving catalyst (Co-OEC) operates from neutral or near neutral water under simply engineered conditions, thus enabling them to be used for direct solar-to-fuels conversion.[5−14] Ex situ[15] and in situ[16] X-ray absorption spectroscopy and attendant atomic pair distribution function analysis[17,18] reveal that self-assembly of the Co-OEC yields a distribution of clusters that is tightly centered about 10(±4) atoms.

Central to the self-assembly process, which forms the basis of the self-repair mechanism of the Co-OEC,[19] is the oxidation of Co^{2+} to Co^{3+} and the role of anion dissociation in this oxidation process, which is indicated by the inverse anion dependence in the electrokinetic rate law for nucleation of the Co-OEC catalyst.[20] In attempting to understand the electron transfer kinetics of Co^{2+} for the Co-OEC self-assembly process, one is confronted with a long-standing and unresolved issue arising from an anomalously high self-exchange rate constant (k_{SE}) of the $Co(OH_2)_6^{3+/2+}$ couple, k_{SE} = 5 M^{-1} s^{-1},[21] which is ∼6 orders of magnitude greater than predictions based on Marcus theory.[22,23] Two proposals have been put forward to account for the anomalous behavior of the $Co(OH_2)_6^{3+/2+}$ self-exchange reaction: a high-spin excited state mechanism[24] and a water-bridging mechanism.[25] By invoking the involvement of a high spin excited state for Co^{3+}, the large reorganization energy associated with a Co^{3+}(low spin)/Co^{2+}(high spin) crossover is minimized. Alternatively, a water bridge between the two cobalt centers has been postulated to facilitate electron transfer by increasing electronic coupling owing to the formation of an inner-sphere complex. In an effort to distinguish between these two disparate mechanisms, temperature-dependent ^{59}Co NMR spectroscopy was undertaken on $Co(OH_2)_6^{3+}$ with the objective of observing a paramagnetic shift, owing to the presence of a high spin state. The absence of such a paramagnetic shift sets a lower limit of 23 kJ/mol for the separation between the high-spin $^5T_{2g}$ excited state and the low-spin $^1A_{1g}$ ground state.[26] Subsequent thermodynamic calculations were in support of this estimation,[27] suggesting the notion that the excited state is too high in energy to participate in the self-exchange reaction at room temperature. Despite this evidence against the excited state mechanism, the water-bridge mechanism, in which the electron transfer takes place through an inner-sphere pathway, remains conjecture, and to date the mechanism for $Co(OH_2)_6^{3+/2+}$ self-exchange electron transfer remains unresolved. Herein, we present the synthesis and characterization of a Co_7 cluster that displays the same cobaltate cluster core as that observed for Co-OEC. The ability to prepare the $Co(II)_7$ and mixed-valent $Co(III)Co(II)_6$ clusters permit a Co(II)|Co(III) self-exchange rate constant to be isolated and measured. An intriguing aspect of the self-exchange reaction is its similarity to the Co(II)|Co(III) couple in a hexaaqua-like O-atom ligand field, but with a secondary structure that precludes the involvement of an inner-sphere electron transfer pathway. By comparing the measured k_{SE} to the calculated k_{SE} using semiclassical Marcus theory, we provide evidence to support the involvement of a water-bridging mechanism for the $Co(OH_2)_6^{3+/2+}$ exchange reaction. Finally, we show that the 6 orders of magnitude discrepancy between

Received: May 4, 2013
Published: August 29, 2013

   dx.doi.org/10.1021/ja404469y | J. Am. Chem. Soc. 2013, 135, 15053−15061

the calculated and measured rate constants for the heptanuclear cluster results from a specific anion interaction with the cluster core. These results provide insight on the role of anions in the self-assembly process of Co-OEC.

EXPERIMENTAL SECTION

General Considerations. *O*-vanillin, methylamine (33 wt % solution in absolute ethanol), methyl-d_3-amine hydrochloride, and triethylamine were purchased from Sigma-Aldrich; $CoCl_2{\cdot}6H_2O$ was purchased from Noah Technologies; and AgOTf and $Zn(OTf)_2$ were purchased from Strem. Acetonitrile-d_3 (1 g ampules) was purchased from Cambridge Isotopes Laboratories, and ^{18}O enriched water (>98%) was purchased from Shanghai Research Institute of Chemical Industry. Commercial reagents were used as received. HL (2-iminomethyl-6-methoxyphenol) was synthesized as described elsewhere.[28] HL* (2-iminomethyl-d_3-6-methoxyphenol) was synthesized in an analogous manner with the exception that CD_3NH_2 was produced by the neutralization of $CD_3NH_2{\cdot}HCl$ with 1 equiv of triethylamine. $Co(OTf)_2{\cdot}(H_2O)_x$ was prepared using a modification of a known procedure.[29] Salt metathesis was accomplished by mixing $CoCl_2{\cdot}6H_2O$ with 2 equiv of AgOTf in deionized water. The AgCl was removed by filtration using Celite on a medium porous frit. The filtrate was concentrated and dried for 24 h in vacuo while agitating with a large stir bar. The resulting pink powder was slightly hydroscopic and therefore stored in a desiccator over $CaSO_4$. The molecular weight of the $Co(OTf)_2{\cdot}(H_2O)_x$ was determined by dissolving known masses in deionized H_2O and back extracting using ε = 4.8 M^{-1} cm^{-1} at λ_{max} = 510 nm for $Co(H_2O)_6^{2+}$.[30] The average of three trials gave a molecular weight of 445 g/mol (very near that of $Co(OTf)_2{\cdot}5(H_2O)$, 447.15 g/mol). This material was then used to prepare a 0.2 M stock solution in 1:1 CH_3CN:H_2O. Complexes **1** and **2** were not significantly moisture or O_2 sensitive; therefore, no attempt was made to exclude water or O_2 during their syntheses. Nonetheless, once synthesized, **1** and **2** were stored in a desiccator over $CaSO_4$. Elemental analyses were performed by Midwest Microlab.

Preparation of $Co_7(OH)_6(L)_6(OTf)_2$ (1). To 20 mL of a 0.20 M solution of $Co(OTf)_2$ in 1:1 MeCN:H_2O (4.0 mmol, 7.0 equiv) was added 20 mL of a 0.17 M solution of HL in MeCN (3.4 mmol, 6.0 equiv). To this was added 943 μL of NEt_3 (6.86 mmol, 12.0 equiv). A deep red solution formed immediately. Slow addition of 5 mL of water induced precipitation of a pink solid. This solid was filtered and washed with 20 mL of 1:3 MeCN:H_2O, then dried in air. This material was dissolved in 80 mL of MeCN and filtered through paper to remove a minor insoluble impurity. The resulting solution was concentrated and dried in vacuo. Yield: 742 mg of pink solid (0.413 mmol, 72.3% yield). ^1H NMR (CD_3CN, δ, all signals are paramagnetically broadened): 59.69 (6H), 57.42 (18H), 47.39 (6H), 13.01 (6H), −13.26 (18H). HR-ESI-MS (m/z): $[M^{2+}-(OTf)_2]$ Calcd for $C_{54}H_{66}N_6O_{18}Co_7$, 749.4873; Found, 749.4868. Anal. Calcd for $C_{56}H_{66}N_6O_{24}S_2F_6Co_7$: C, 37.41; H, 3.70; N, 4.67. Found C, 37.15; H, 3.69; N, 4.44.

Preparation of $Co_7(OH)_6(L^*)_6(OTf)_2$ (1*). The labeled complex was prepared in the same manner as **1**, but at half scale, using HL* in place of HL. Yield: 343.1 mg of pink solid (0.1889 mmol, 66.53%). ^1H NMR (CD_3CN, δ, all signals are paramagnetically broadened): 59.69 (6H), 57.42 (18H), 47.39 (6H), 13.01 (6H). HR-ESI-MS (m/z): $[M^{2+}-(OTf)_2]$ Calcd ($C_{54}H_{48}D_{18}N_6O_{18}Co_7$) 758.5438; found 758.5414. Anal. Calcd for $C_{56}H_{48}D_{18}N_6O_{24}S_2F_6Co_7$: C, 37.04; H, 3.66; N, 4.63. Found C, 37.34; H, 3.72; N, 4.70.

Preparation of $Co_7(OH)_6(L)_6(OTf)_3$ (2). To a solution of **1** (172.6 mg, 0.9600 mmol) in 10 mL of nitromethane was added AgOTf (24.7 mg, 0.0960 mmol) in 630 μL of nitromethane. The mixture was stirred overnight at 40 °C, by which time a silver mirror had formed. The solution was filtered through a combination of Celite and glass wool to remove finely divided Ag^0, then concentrated and dried in vacuo. Yield: 180.8 mg of brown solid (0.09287 mmol, 96.74%). ^1H NMR (CD_3CN, δ, all signals are paramagnetically broadened): 70.98 (18H), 60.55 (6H), 55.08 (6H), 20.91 (18H), 10.67 (6H). HR-ESI-MS (m/z): $[M^{2+}-(OTf)]$ Calcd for $C_{55}H_{66}N_6O_{21}SF_3Co_7$, 823.9639; Found, 823.9607. Anal. Calcd for $C_{57}H_{66}N_6O_{27}S_3F_9Co_7$: C, 35.16; H, 3.42; N, 4.32. Found C, 35.24; H, 3.43; N, 4.40.

Preparation of $Zn_7(OH)_6(L)_6(OTf)_2$ (3). **3** was prepared in an analogous fashion to **1**, replacing $Co(OTf)_2$ with $Zn(OTf)_2$ but at a 15% scale. Yield: 122.6 mg of pale yellow solid (0.06647 mmol, 77.55%). ^1H NMR (CD_3CN, δ): 8.295 (6H, d), 7.025 (6H, dd), 6.95 (6H, dd), 6.66 (6H, t), 3.63 (18H, s), 3.31 (18H, d) 1.55 (6H, s). HR-ESI-MS (m/z): $[M^{2+}-(OTf)_2]$ Calcd for $C_{54}H_{66}N_6O_{18}Zn_7$, 771.9684. Found, 771.9662. Anal. Calcd for $C_{56}H_{66}N_6O_{24}S_2F_6Zn_7$: C, 36.50; H, 3.61; N, 4.56. Found C, 36.78; H, 3.60; N, 4.38.

Physical Measurements. NMR spectra were recorded at the MIT Department of Chemistry Instrumentation Facility on a Varian Inova-500 NMR Spectrometer. ^1H NMR spectra were referenced to the residual proteo solvent resonances. ^{19}F NMR spectra were referenced to $CFCl_3$. Vis-NIR spectra were recorded at 293 K, and samples were prepared in air using acetonitrile previously dried by passage through an alumina column under argon. Extinction coefficients were determined by averaging spectra from nine individually massed samples. IR spectra were recorded on PerkinElmer Spectrum 400 FT-IR/FT-FIR spectrometer. Solid samples were acquired using a Pike Technologies GladiATR attenuated total reflectance accessory with a monolithic diamond crystal stage and pressure clamp. Solution IR measurements were made using KBr windows in a semipermanent liquid cell. Magnetic measurements were performed at the MIT Center for Materials Science and Engineering Shared Experimental Facility on a Quantum Design Magnetic Properties Measurement System (MPMS-XL). Solution magnetic measurements were performed using the Evans method in acetonitrile with benzene as the indicator. In both cases, diamagnetic corrections were applied using Pascal's constants.[31] Mass spectrometry was conducted on a Bruker Daltonics APEXIV 4.7 T FT ion cyclotron resonance mass spectrometer using an electrospray ionization source (ESI). Mass spectrometry samples were run in neat acetonitrile, and the data were processed using the program mMass Version 4.0.

Kinetics Measurements. Samples of **1*** and **2** were separately dissolved in 500 μL of acetonitrile-d_3 (CD_3CN). The total solvent volume was 1 mL to avoid precipitation, which was sometimes observed at lower volumes. The Varian Inova-500 NMR spectrometer was equipped with a variable temperature controller, which maintained the temperature within ±0.1° the desired temperature. Once at temperature, the probe was tuned using a 1 mL of blank CD_3CN sample in a J-Young tube identical to that used for the sample. The solutions of **1*** and **2** were mixed, added to a J-Young tube, and firmly sealed. The sample was locked and shimmed, a process that allowed ample time for the sample to equilibrate to the set temperature. The kinetics run was programmed using the array function with a preacquisition delay, which was adjusted depending on the temperature. Each FID was composed of 16 transients with a 0.3 s acquisition time (at) and a first delay (d1) of 4 s. The spectral window was expanded to include all peaks. All other parameters were the same as a default proton spectrum. Upon completion of the kinetics run, a NMR spectrum of the sample was acquired on a Varian Inova-500 NMR spectrometer with an inverse broadband probe for enhanced proton sensitivity. From this spectrum, an accurate ratio of C_1/C_2, where C_1 = [**1**] + [**1***] and C_2 = [**2**] + [**2***] was measured by integration of the nonexchanging peaks near 11 ppm. Independent measurements of these peaks with known amounts of **1** and **2** confirmed the validity of this method. The sample was then diluted once with CD_3CN, and a vis-NIR spectrum was recorded to measure the total absorbance at λ_{max} ~ 666 nm. From the NMR ratio and the known extinction coefficients of **1** and **2**, the concentrations C_1 and C_2 were determined by solving two equations with two unknowns. Due to practical experimental restraints, such as time of measurement and solubility, C_1 and C_2 were held within a range of 4−11 mM. The rate of electron transfer, R_{ET}, was measured by applying the MacKay equation,

$$-\ln\left(1-\frac{[\mathbf{1}]_t}{[\mathbf{1}]_\infty}\right)=\frac{R_{ET}(C_1+C_2)}{C_1\cdot C_2}t \qquad (1)$$

dx.doi.org/10.1021/ja404469y | J. Am. Chem. Soc. 2013, 135, 15053−15061

to the scrambling of the deuterium labeled between **1*** and **2**.[32,33] The progress of the reaction was conveniently monitored by tracking the increase of the signal from [**1**] at −10 ppm. The rate constant was found by fitting the $[\mathbf{1}]_t$ versus time to a monoexponential function using the program Origin, which resulted in R^2 values of 0.985 or greater. Assuming $R_{ET} = k_{obs}C_1C_2$, the rate constant is given by,[34]

$$k_{obs} = \frac{1}{\tau(C_1 + C_2)} \quad (2)$$

X-ray Crystallographic Details. **1** and **2** co-crystallized from a mixture of **1*** (15.5 mg) and **2** (13.3 mg) in 1 mL of CD_3CN, which was left undisturbed at room temperature for 2 weeks. Large block-shaped crystals of brown/orange color were collected, and a large single crystal was mounted on a Bruker three circle goniometer platform equipped with an APEX detector. A graphite monochromator was employed for wavelength selection of the Mo Kα radiation (λ = 0.7103 Å). The data were processed and refined using the program SAINT supplied by Siemens Industrial Automation. Structures were solved using direct methods in SHELXS and refined by standard difference Fourier techniques in the SHELXTL program suite (6.10 v., Sheldrick G. M., and Siemens Industrial Automation, 2000). Hydrogen atoms bound to carbon atoms were placed in calculated positions using the standard riding model and refined isotropically. The oxygen-bonded hydrogen atoms were located in the difference map, and distances were restrained to 0.84 Å. The isotropic displacement parameters of these hydrogen atoms were fixed to 1.2 times the U value of the oxygen atoms to which they were bonded. All non-hydrogen atoms were refined anisotropically. The structure contained a disordered triflate anion and acetonitrile solvate molecule, which occupied the same space adjacent to an inversion center. This disorder was satisfactorily modeled using the Part 1 and Part 2 commands and a site occupancy factor of 0.5. The 1,2-distances and 1,3-distances of the disordered molecules were restrained to be similar using the SAME command, and the rigid bond restraints SIMU and DELU were applied. Hydrogen bonding parameters were calculated using the HTAB command. Unit cell parameters, morphology, and solution statistics for the structures are summarized in Table S1. All thermal ellipsoid plots are drawn at the 50% probability level with carbon-bound hydrogen atoms and solvent molecules omitted for clarity.

RESULTS

Synthesis and Characterization of 1 and 2. The choice of 2-iminomethyl-6-methoxy-phenol (HL) for stabilizing a cobaltate cluster core was motivated by the synthetic method of Zhou et al. that delivers the perchlorate salt of **1**.[35] The reaction proceeded at a maximal yield of 45.9% using nonstoichiometric reagents under microwave reactor conditions, as an alternative to traditional hydrothermal synthetic methods. Given the fast ligand exchange rates for the Co(II) ion,[36] we surmised that by utilizing the precise stoichiometry of 7:6:12 Co/HL/NEt_3, we would be able to cleanly synthesize the desired product at ambient temperatures, as summarized in Figure 1 (top). Indeed, under these conditions and at room temperature, we found that the triflate salt of **1** precipitated from MeCN:H_2O solutions when the water content was raised above 25%. An elementally pure compound was isolated by simple filtration to remove a minor insoluble impurity. The universality of this procedure was confirmed by its successful implementation in the synthesis of **3**, the analogous zinc cluster $Zn_7(OH)_6(L)_6(OTf)_2$, which was previously crystallographically characterized as the nitrate salt.[28]

The identification of optimum reaction conditions was aided by the distinct NMR spectra exhibited by these compounds. Consistent with the S_6 symmetry of the complexes, only one set of ligand resonances was observed. The NMR spectra for all compounds are presented in Figures S1−S5. The spectrum for

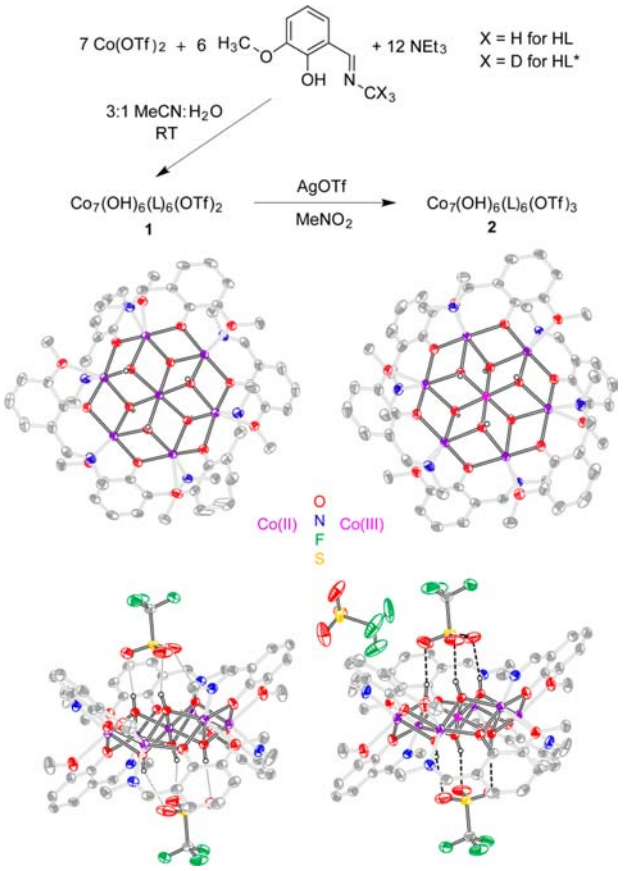

Figure 1. (top) Synthetic scheme of compounds **1** (left) and **2** (right). Thermal ellipsoid plot for **1** and **2** with ellipsoids shown at the 50% probability level: (middle) top-down view with triflate anions removed for clarity and (bottom) side-on view with all anions shown and hydrogen bonds drawn as dotted lines or dashed lines.

1 (Figure S1) exhibits broadening and paramagnetic shifts of the signals due to the presence of the high spin Co(II) ions. All but the aldiminic and hydroxide proton resonances were observable. For **3**, a diamagnetic compound, all proton resonances were observed (Figure S5) and they exhibited the expected shifts and couplings.

The oxidation of **1** to **2** proceeded cleanly using the oxidant AgOTf in nitromethane, which solubilizes **1**, **2**, and AgOTf and ensures the full oxidizing potency of the Ag^+ ion.[37] The formal potential for the **1**/**2** couple was estimated by cyclic voltammetry (CV). The CVs of **1** and **2** at room temperature and in the presence of 0.1 M TBAOTf (Figure S6) exhibit broad, electrochemically irreversible waves. The oxidation of **1** occurs between 0.4 and 0.6 V while the reduction of **2** occurs between −1.0 and −1.2 V (E_{pa} = 0.487 V and E_{pc} = −1.099 V, all potentials vs $Fc^{+/0}$). The formal potential cannot be deduced without more detailed electrochemical experiments, but it can be bracketed as <0 V, which is consistent with the observation that treatment of **1** with 1.5 eq of FcOTf results in conversion to **2**, as observed by NMR (Figure S9).

Complexes **1** and **2** co-crystallize from a solution mixture and they were characterized using X-ray diffraction analysis. The thermal ellipsoid plots are presented in Figure 1. A bond contraction of 0.174 Å between the central cobalt atom, Co(1), and the surrounding μ_3-OH ligands is observed upon oxidation. The bond contraction is consistent with a localized Co(III) valency at Co(1) in **2**, as has been observed in a related

dx.doi.org/10.1021/ja404469y | J. Am. Chem. Soc. 2013, 135, 15053−15061

structure containing the same $Co(III)Co(II)_6(OH)_6$ cluster core stabilized by six iminophenyl-methoxyphenol ligands.[38] A comparison between **1** and **2** of the cobalt atoms' inner sphere bond distances is presented in Table 1 (see Figure S20 for an overlay of the structures). The bond lengths associated with the outer cobalt atom, Co(2), change only modestly; the average Co(2)−O/N bond lengths are 2.11 ± 0.15 Å for both clusters. The contraction of the hydroxides around the central Co(1) of **2** results in a bond lengthening between the hydroxide ligands and the outer cobalt atoms, Co(2). The lengthening is asymmetric with a 0.073 Å increase for the bond trans to the more electron donating imine group and only 0.024 Å longer for the bond trans to the weakly donating methoxy moiety. The remaining bonds to the Co(2) atoms contract to compensate for the lost electron density from the hydroxides, but these contractions are slight (≤0.037 Å) owing to the rigidity of the six iminomethyl methoxyphenol ligands, L^-.

Table 1. Comparison of Inner Sphere Bond Lengths[a]

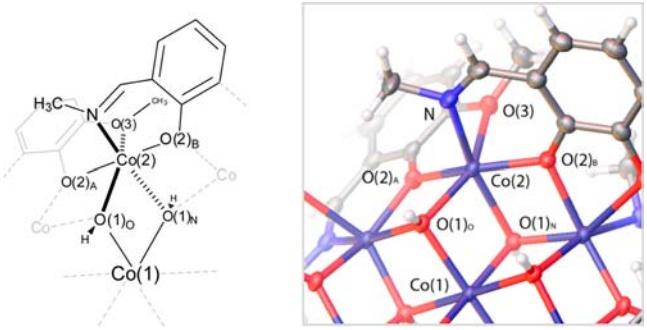

bond	**1** d_0 (Å)	**2** d_0 (Å)	Δd_0 (Å)
Co(1)−O(1)	2.092(11)	1.918(1)	−0.174(11)
$Co(2)-O(1)_N$	2.149(16)	2.219(24)	0.070(29)
$Co(2)-O(1)_O$	2.016(3)	2.0393(6)	0.024(4)
$Co(2)-O(2)_A$	1.995(9)	1.969(2)	−0.026(9)
$Co(2)-O(2)_B$	2.051(11)	2.014(4)	−0.037(12)
Co(2)−O(3)	2.395(32)	2.367(18)	−0.028(37)
Co(2)−N	2.077(2)	2.056(8)	−0.021(8)

[a]Averaged over three crystallographically independent bonds found in the asymmetric unit. Error calculated using one standard deviation from the average and propagated in the usual way.[39]

The $Co_7(OH)_6$ cores of **1** and **2** are coordinated by triflate anions via hydrogen bonding interactions. One triflate anion occupies each bowl-shaped cavity (two per molecule) created by the ligand architecture, and each anion makes a three-point hydrogen bond with the protons of the μ_3-OH bridging ligands. A fifth anion is associated with the oxidized cluster **2** but remains outside the cavities and does not act as a hydrogen bond acceptor. The donor−acceptor (D···A) distances between the triflate anions and the μ_3-OH of **2** are 2.855(3), 2.870(3), and 2.942(3) Å (dashed lines), whereas the interaction with **1** is much weaker as indicated by the significantly longer D···A distances; 3.005(3), 3.043(4), and 3.063(3) Å (dotted lines).

Three different analyses were performed to understand the interaction of triflate with **1** and **2** in solution. First, ESI mass spectra were examined to assess the stability of anion-bound complexes in acetonitrile solutions. Figure S7 shows the observed and calculated mass spectra for **1** and **2** in acetonitrile. The most intense signal in the spectrum of **1** appears at 758.54 m/z, corresponding to the anion-bare cluster, $Co_7(OH)_6(L)_6^{2+}$, whereas in the spectrum of **2**, the strongest signal observed appears at 823.97 m/z and corresponds to the triflate-bound $Co_7(OH)_6(L)_6(OTf)^{2+}$. The m/z signature for the anion-bare $\mathbf{2}^{3+}$ was observed, but has a 10% relative intensity compared to the anion-bound $\mathbf{2}OTf^{2+}$.

Second, ^{19}F NMR was used to probe the chemical environments of the triflate anions in the clusters. Despite the paramagnetic behavior of **1** and **2**, clear ^{19}F signals were observed (Figure S11). At room temperature, the triflate signal for **2** is shifted 9.16 ppm upfield of **1**, which itself is very near to free triflate in an acetonitrile solution of TBAOTf. The linewidths of both spectra are broadened relative to TBAOTf (3.93 Hz), with a significantly increased broadening in **2** (27.12 Hz) as compared to **1** (9.49 Hz). The broadening in **2** cannot be attributed to paramagnetism alone because it is less paramagnetic than **1**, which shows a sharper line width. Figure 2 presents the NMR for samples that were cooled to −40 °C to explore the possibility of chemical exchange. With decreasing temperature, an increased broadening of the ^{19}F signal and a downfield shift were observed in **2**, whereas the line width for **1** changes only slightly with no noticeable perturbation of the chemical shift. This is consistent with fast exchange between inequivalent triflate anions in **2**, but not in **1**, and because the shift in **2** is downfield, toward the signal for "free" triflate, it suggests that two of the three triflate anions are less influenced by the chemical environment of the cluster than the third.

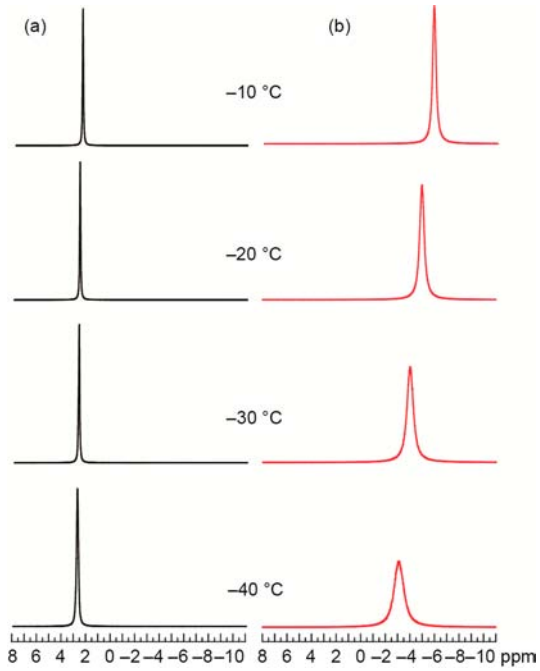

Figure 2. ^{19}F NMR spectra at 500 MHz, in the temperature range indicated of (a) **1**, 8 mM in CD_3CN and (b) **2**, 10 mM in CD_3CN. Spectra were referenced to TBAOTf in CD_3CN.

Finally, the O−H stretching energies of **1** and **2** were analyzed in solution and in the solid state by IR spectroscopy. The data are presented in Figure S8. The IR spectrum of co-crystals of **1** and **2** contains peaks at 3580 cm^{-1} and 3462 cm^{-1}, assigned to **1** and **2**, respectively. These stretches match well with independent solid samples of **1** and **2**. In solution, the large separation between the major peaks is maintained and even increases slightly due to an approximate 60 cm^{-1} shift to lower energy in the spectrum of **2**. In both solution spectra, the

dx.doi.org/10.1021/ja404469y | J. Am. Chem. Soc. 2013, 135, 15053−15061

presence of high energy shoulders suggests asymmetric hydrogen bonding.

The magnetic properties of **2** were investigated in the solid state by SQUID magnetometry and in solution by the variable temperature Evans method.[40,41] The data are presented in Figure S10. The magnetism of the perchlorate salt of **1** was previously reported.[35] The room temperature $\chi_M T$ value for **2** was 16.3 $cm^3\ mol^{-1}$ K as measured by the Evans method; this is approximately 4.5 $cm^3\ mol^{-1}$ K less than that measured for **1**. The slow increase in $\chi_M T$ with decreasing temperature is suggestive of weak intramolecular ferromagnetic exchange between Co(II) ions and is consistent with data from **1** and other disc-like heptanuclear clusters.[35,42] Importantly, these magnetic data indicate that Co(1) in **2** has a low-spin electronic configuration and that a spin equilibrium, which is known for Co(III) ions in weak oxygen-atom ligand fields,[43] is not operable within this temperature range.

Self-Exchange Kinetics. The rate of electron transfer between **1*** and **2** in MeCN with no added electrolyte was studied over the temperature range of 40−70 °C. To ensure that only electron transfer and not ligand substitution resulted in the productive transfer of the label from **1*** to **2***, control experiments were performed in which **1*** and **2*** were separately treated with **3** for 18 h at 50 °C. Co(II) and Zn(II) ions have similarly fast ligand exchange rates,[36] so the lack of ligand scrambling between **3** and **1*** or **2*** (Figure S12) provided assurance that, within the temperature range of the study, only electron transfer was responsible for the apparent transfer of L*. Representative traces of the raw NMR data at 40 °C and the subsequent monoexponential fit are shown in Figure 3. The average of two kinetic runs at this temperature resulted in a k_{obs} = 1.53 × 10^{-3} $M^{-1}\ s^{-1}$ at 38 mM total concentration of triflate, $[OTf]_{total}$. As the reaction temperature was raised, the rate constant increased to 2.93 × 10^{-2} $M^{-1}\ s^{-1}$ at 70 °C and 21 mM $[OTf]_{total}$. The temperature dependent data, plotted in the Eyring form, are presented in Figure 4. The data exhibit excellent linearity, and a least-squares fit produces a R^2 = 0.99 with a slope of 12 200 ± 300 K and intercept of 27 ± 1 $\ln(M^{-1}\ s^{-1})$.

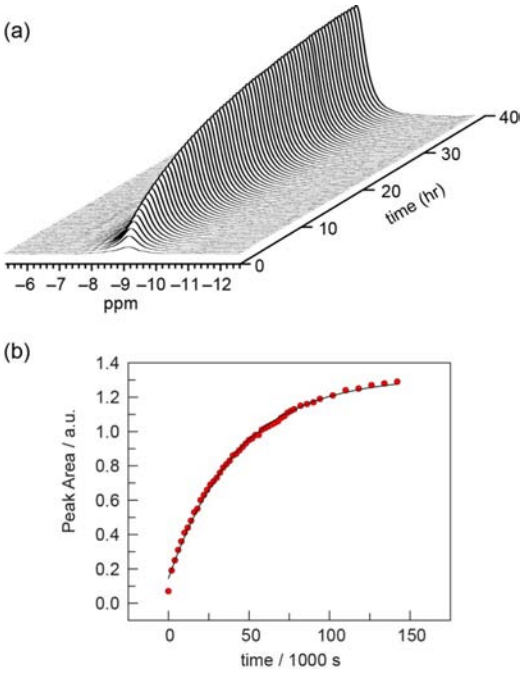

Figure 3. (a) Representative stacked plot of the increase in ^{1}H methyl iminium signal during a kinetics measurement at 40 °C in MeCN, $[C_1]$ = 8.65 mM and $[C_2]$ = 6.21 mM. (b) The integration of the signal versus time and subsequent monoexponential fit to furnish τ = 43 100 ± 900 s.

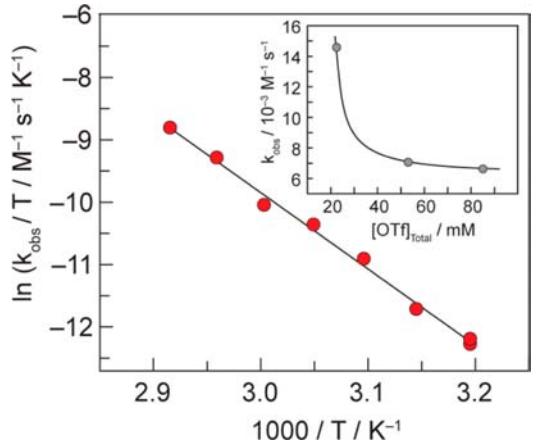

Figure 4. Temperature dependence of the observed rate constant in MeCN, plotted in the Eyring form, $\ln(k_{obs}/T)$ vs $1/T$. The average $[OTf]_{Total}$ = 30 ± 10 mM. The linear fit yields a slope of −12200 ± 300 K and intercept of 27 ± 1 $\ln(M^{-1}\ s^{-1})$. (Inset) Dependence of k_{obs} at 60 °C on the concentration of triflate from all sources, $[OTf]_{Total}$ = $[OTf]_1$ + $[OTf]_2$ + $[OTf]_{TBAOTF}$. The line is presented merely as a guide.

The anion dependence on k_{obs} was probed at 60 °C. Due to solubility concerns, the highest concentration of TBAOTf that could be added was 60 mM. An inhibitory effect of the anion was observed; k_{obs} decreased by a factor of 2 (inset, Figure 4) as the total concentration of triflate was raised from 22 mM to 85 mM.

DISCUSSION

Electron Transfer Rate Calculations. The theoretical self-exchange rate constant at 40 °C was calculated using semiclassical Marcus theory for a comparison to the experimental value:[22,44]

$$k_{ET} = K_A \upsilon_n \kappa_{el} \exp\left[\frac{-[\Delta G^*_{out} + \Delta G^*_{in}(T)]}{RT}\right] \quad (3)$$

$$K_A = 4\pi N r^2 \delta r \exp\left(\frac{-w(r)}{RT}\right) \quad (4)$$

$$w(r) = \frac{N z_2 z_3 e^2 \exp[\beta(\sigma - r)\sqrt{\mu}]}{4\pi\varepsilon_0\varepsilon_r r(1 + \beta r\sqrt{\mu})} \quad (5)$$

$$\Delta G^*_{in}(T) = \frac{N}{2}\sum f_i \left(\frac{\Delta d_0}{2}\right)^2 \frac{4kT}{h\upsilon_i} \tanh \frac{(h\upsilon_i)}{4kT} \quad (6)$$

$$\Delta G^*_{out} = \frac{N\Delta q^2}{16\pi\varepsilon_0}\left(\frac{1}{2a_2} + \frac{1}{2a_3} - \frac{1}{r}\right)\left(\frac{1}{n_D{}^2} - \frac{1}{\varepsilon_r}\right) \quad (7)$$

$$\upsilon_n = \left(\frac{\upsilon_i{}^2 \Delta G^*_{in}}{\Delta G^*_{out} + \Delta G^*_{in}}\right)^{1/2} \quad (8)$$

dx.doi.org/10.1021/ja404469y | J. Am. Chem. Soc. 2013, 135, 15053−15061

Initially, we assume that the electron transfer is adiabatic and thus the electronic factor, $\kappa_{el} = 1$. As Sutin has emphasized, though Co(II)|Co(III) exchanges are formally spin forbidden and therefore should be inherently nonadiabatic, comparisons of observed rate constants to calculated rate constants do not allow for any special nonadiabaticity.[45] The nuclear tunneling correction is applied because of the large change in the bond distance at the Co(1) atom. Even at high temperatures, this correction can result in a significant decrease in the free energy of inner sphere reorganization, ~4 kJ/mol for $\Delta d_0 = 0.17$ Å.[46]

The crystal structure of **1** co-crystallized with **2** is used as a representation of the reactants in a precursor complex and, conveniently, many input parameters for eqs 3−8 are deduced from it directly. To begin, we assume that only the largest bond distance changes, Co(1)−O(1) and Co(2)−O(1), in Table 1 play a dominant role in the inner sphere reorganization energy. The average breathing frequencies, υ_i, are estimated from vibrational data to be 425 cm^{-1} and 366 cm^{-1}, respectively (Figure S15). Using these values, the inner sphere reorganization energy was calculated using eq 6, $\Delta G_{in}^*(T) = 50.9$ kJ/mol. The hard sphere radii of the reactants, a_2 and a_3, and the center-to-center distance, r, were measured for nearest neighbor pairs and found to be $a_2 = a_3 = 6.6$ Å and $r = 12.2$ Å (see SI for details on the calculations of a_2 and a_3 and Figures S16−19 for depictions of measurements). Using these metrics and known physical constants for acetonitrile,[47] $\Delta G_{out}^* = 12.7$ kJ/mol is evaluated from eq 7. This value is ~2 times smaller than many Co(II)|Co(III) couples, traditionally studied in water, owing to the lower dielectric constant for acetonitrile and the large sizes of **1** and **2**.[48]

The equilibrium constant for a precursor complex (K_A) is given by eq 4 and includes a work contribution, which is dependent on ionic strength. The importance of the work term is illuminated by the dependence of the observed rate constant on electrolyte concentration (Figure 4, inset). Debye−Hückel theory predicts that, for similarly charged species, increasing the ionic strength will increase the rate constant by decreasing the magnitude of the work term.[49] Also, the rate constant for electron transfer may be further influenced to the extent that higher ionic strength may increase the ion pairing of reactants and their counterions. Indeed, self-exchange and cross-exchange studies in acetonitrile have shown the expected increase in rate constant with increasing electrolyte concentration when the reactants are of like charge.[50,51] Since electrolyte had an inhibitory effect in this study, it is reasonable to assume that at the concentrations employed, there is sufficient ion pairing to make the work term negligible or at least small enough that other processes, which are inversely dependent on anion, are more influential. With the assumption that $w(r)$ is negligible, the equilibrium constant was calculated, $K_A = 0.9$ M^{-1}. If the work term is included, the equilibrium constant is reduced by a factor of 14 to $K_A = 0.06$ M^{-1}, i.e., when assuming no ion pairing and an ionic strength of $\mu = 68$ mM (the average of the 40 °C trials). The rate constant at 40 °C is $k_{SE}(calc) = 3 \times 10^2$ M^{-1} s^{-1} using $K_A = 0.9$ M^{-1}, the reorganizational energies mentioned previously, and a nuclear vibrational frequency ($\upsilon_n = 10^{13}$ s^{-1} from eq 8). This calculated rate constant is 5 orders of magnitude higher than the observed value. Even with a large work term included, $k_{SE}(calc) = 3 \times 10^1$ M^{-1} s^{-1}. Thus, $k_{SE}(obs)$ is considerably smaller than what is expected for any experimental condition invoked for an adiabatic electron transfer.

Evidence for the Mechanism of Hexaaqua Self-Exchange ET. A comparison of the observed k_{SE} for **1**|**2** self-exchange and $Co(OH_2)_6^{3+/2+}$ relative to those calculated by Marcus theory provides insight into the mechanism of Co(II)|Co(III) self-exchange. Compounds **1** and **2** retain the hexaaqua-like O-atom ligand field, but unlike $Co(OH_2)_6^{3+/2+}$, these compounds possess a secondary coordination structure that precludes electron transfer by an inner-sphere pathway. Conversely, **1** and **2** are electronically similar to $Co(OH_2)_6^{3+/2+}$ owing to similar ligand fields, and therefore the participation of excited states, if they are important to Co(II)|Co(III) self-exchange, will prevail in either system. In this case, both **1** and **2** and $Co(OH_2)_6^{3+/2+}$ would be expected to have inflated k_{SE} relative to that predicted by Marcus theory. Conversely, k_{SE} of **1**|**2** should be slower than a Marcus-predicted rate constant owing to the steric clashing of the cluster cores (and attendant six chelating ligands) and the coordinative saturation of Co(1) whereas k_{SE} of $Co(OH_2)_6^{3+/2+}$ should be greater than a Marcus-predicted rate constant owing to the facility of inner-sphere complex formation, as originally proposed by Endicott and co-workers.[25]

In assessing the participation of excited states, and in particular, the high-spin $^5T_2$ excited state in Co(II)|Co(III) self-exchange electron transfer, a ligand field analysis is useful. Because the ligand environments of the periphery Co(II) ions are similar in both **1** and **2**, the absorption profiles in the visible range are nearly identical for the two molecules (Figure S13). The d−d transitions of the Co(III) atom in **2** are obscured by those of the neighboring Co(II) atoms, and thus identification of the $^5T_2$ excited state in **2** is obstructed. Notwithstanding, the structural metrics of **2** support the conjecture of a weak, and likely weaker, ligand field for Co(III) in **2** than that for Co(III) residing in a hexaaqua environment. The Co(II) → Co(III) bond distance contraction of 0.174 Å (Table 1) is much smaller than the 0.21 Å contraction seen for the hexaaqua complex.[52] Furthermore, the interaction of the Co(1) atoms with the μ_3-OH ligands will polarize electron density away from putative Co(2) bonding interactions. A similar interaction between La and O ions occurs in the solid-state material, $LaCoO_3$.[53] In $LaCoO_3$, this polarization stabilizes the intermediate and high-spin excited states of the Co(III) ion with respect to the low-spin ground state, resulting in a nonzero bulk magnetic moment at temperatures above 100 K.[54,55] Together, the longer metal ligand bonds and polarization effect suggest that a weaker ligand field is expected for Co(III) in **2**, and correspondingly the $^5T_2$ excited state should be to lower-energy than in $Co(OH_2)_6^{3+}$. Though the involvement of a high-spin excited state of **2** would be more probable than for $Co(OH_2)_6^{3+}$, the k_{SE} for **1**|**2** self-exchange is exceptionally small, indicating that the excited state does not mediate electron transfer. In this regard, these results support the notion that a water-bridging mechanism is operable and explains the very high Co(II)|Co(III) self-exchange rates of $Co(OH_2)_6^{3+/2+}$.

Origins of Slow Electron Transfer. While the water-bridged mechanism explains the fast Co(II)|Co(III) self-exchange rate of $Co(OH_2)_6^{3+/2+}$, it does not account for the exceptionally slow **1**|**2** self-exchange reaction. In the absence of an inner sphere mechanism, Marcus theory predicts a k_{SE} that is 5 orders of magnitude greater than the observed rate constant.

$$k_{obs} = \frac{k_B T}{h} \exp\left(-\frac{\Delta H^{\ddagger}}{RT}\right) \exp\left(\frac{\Delta S^{\ddagger}}{R}\right) \quad (9)$$

dx.doi.org/10.1021/ja404469y | J. Am. Chem. Soc. 2013, 135, 15053−15061

The temperature dependence of the rate constant provides evidence as to the source of the discrepancy. An analysis of the slope of Figure 4 using eq 9 results in an experimental activation enthalpy of 99 ± 1 kJ/mol, which is 35 kJ/mol larger than the value calculated using eqs 6 and 7. This increased enthalpy is more than enough to account for a 10^5 difference between the experimental and calculated rate constant. Thus, the discrepancy between k_{obs} and k_{calc} appears to arise from an underestimation of the enthalpy of activation. With an excellent model of the precursor complex provided by the crystal structure, the activation parameters, $\Delta G(T)_{in}$ and ΔG_{out}, are calculated with good assurance. However, a larger enthalpy of activation is expected if electron transfer is attendant to movement of a hydrogen-bonded triflate anion. The inhibitory effect of counterion movement on ET rate constants has been recognized for both intra- and intermolecular ET in organic solvents.[56,57] Given that the crystal structures imply a preference for triflate association to $\mathbf{2}^{3+}$ and ^{19}F NMR, ESI-MS, and IR data of **2** indicate anion association is preserved in solution, it is expected that the dominant solution species for the oxidized cluster is $[\mathbf{2}OTf]^{2+}$. A model for self-exchange electron transfer between the thermodynamically stable solution species that accounts for anion association is depicted in Scheme 1. Whereas ^{19}F NMR indicates fast triflate exchange

Scheme 1

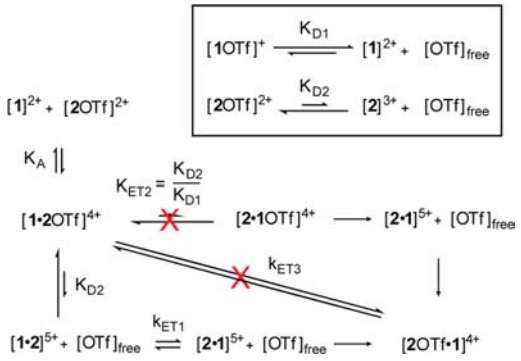

on the NMR time scale, electron transfer is slow on this timescale. The electron transfer step is therefore expected to be rate-limiting in all cases. For this reason, we consider only anion dynamics that precedes or accompanies electron transfer, thus simplifying the kinetic analysis.[58]

The relevant rate expression for ET is:

$$R_{ET} = k_{ET1}[\mathbf{1}^{2+}][\mathbf{2}^{3+}] + k_{ET2}[\mathbf{1}^{2+}][\mathbf{2}OTf^{2+}] + k_{ET3}[\mathbf{1}^{2+}][\mathbf{2}OTf^{2+}] = \frac{k_{ET1}(K_{D2}/[OTf]_{free}) + k_{ET2} + k_{ET3}}{(K_{D2}/[OTf]_{free} + 1)} C_1 C_2 \quad (10)$$

and, acknowledging $K_{D2} \ll [OTf]_{free}$, then the observed rate constant becomes,

$$k_{obs} = k_{ET1}\frac{K_{D2}}{[OTf]_{free}} + k_{ET2} + k_{ET3} \quad (11)$$

All three terms of eq 11 are expected to give observed enthalpies of activation that exceed that predicted from Marcus theory, albeit, for difference reasons. Electron transfer at the nuclear configuration of the precursor complex $[\mathbf{1}{-}\mathbf{2}OTf]^{4+}$, k_{ET2}, will be thermodynamically uphill by the value determined from the ratio of the anion dissociation constants:

$$\Delta G^{\circ}_{ET2} = -RT \ln \frac{K_{D2}}{K_{D1}} \quad (12)$$

which, since experimental data suggests $K_{D2}/K_{D1} \ll 1$, is expected to be significant. Electron transfer that is concerted with anion transfer, k_{ET3}, will be thermoneutral but will have an increased reorganizational energy due to the movement of the anion, eq 13.[59]

$$\Delta G^{\ddagger}_{ET3} = \Delta G^{*}_{in} + \Delta G^{*}_{out} + \Delta G^{*}_{anion} \quad (13)$$

Finally, electron transfer that follows a fast anion pre-equilibrium, k_{ET1}, will result in a higher observed enthalpy of activation because the measured value will encompass the enthalpic component of both steps, anion dissociation and electron transfer, eq 14.

$$\Delta G^{\ddagger} = \Delta G^{*}_{ET1} + \Delta G^{\circ}_{K_{D2}} \quad (14)$$

However, only this first term of eq 11 can account for the observed decrease in k_{obs} with increasing triflate concentration. Thus, at the concentrations explored, the pathway that accounts for the observed scrambling of the deuterium label is a facile anion dissociation pre-equilibrium from $\mathbf{2}OTf^{2+}$ to give a precursor complex for which rate-limiting electron transfer proceeds with $\Delta G^{\circ}_{ETI} = 0$ (Scheme 2).

Scheme 2

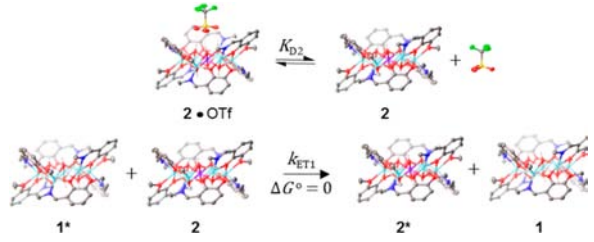

Since the electron transfer is between spin-orthogonal cobalt atoms that are separated by 12.2 Å, the electronic factor, κ_{el}, is expected to be much less than 1; that is, the electron transfer should be nonadiabatic. Nevertheless, as has been observed with other Co(II)|Co(III) couples,[45] the slow observed rate constant measured in this study can be accounted for by a large enthalpy of activation. The experimentally derived preexponential term, assuming no contribution due to entropy from inner or outer reorganization energies, is,

$$K_A \upsilon_n \kappa_{el} = \frac{k_{obs}}{\exp(-\Delta H^{\ddagger}/RT)} (\text{at } 313 \text{ K}) = 5 \times 10^{13}\ \text{M}^{-1}\ \text{s}^{-1} \quad (15)$$

which is within an order of magnitude of the calculated preexponential term assuming $\kappa_{el} = 1$. The effect of non-adiabaticity may be slight or hidden by a counter-balancing of a positive entropy component, which could be expected for a dissociation mechanism.

Anion-mediated electron transfer provides a molecular basis for the observed inverse first-order dependence on buffer in the mechanism of Co-OEC catalyst self-assembly. The electro-kinetic model for nucleation shows that phosphate inhibits film growth.[20] We originally suspected that the anion dependence found its origin in ligand substitution, where the anion would

have to be substituted for cluster self-assembly. However the studies described herein suggest that the anion may also modulate the kinetics of electron transfer. Since the growth of thick films must proceed with charge transport through an already deposited film, we envision a self-exchange mechanism proceeding between neighboring Co-OEC clusters. Hydrogen bonded anions could stabilize the hole with respect to Co(II) oxidation. Since this electron transfer is likely to be slow and does not involve the transfer of an electron to the electrode, it is possible that this final electron transfer is the rate-determining chemical step derived from the electrochemical rate law.

CONCLUSION

In summary, an improved synthesis of disc-shaped heptanuclear cobalt hydroxide model compound has been extended to the preparation of an analogous zinc complex. The one-electron oxidized cobalt compound features a localized Co(III) valency in a weak, oxygen atom ligand field. The self-exchange electron transfer rate constant as measured by isotope exchange is anomalously slow as compared to that predicted from semiclassical Marcus theory. The discrepancy in observed and calculated rates supports a charge transfer mechanism that requires anion dissociation from the oxidized cluster before electron transfer can occur. This mechanism sheds light on the inverse dependence of anions in the self-repair mechanism of Co-OECs. Moreover, because H_2O cannot directly bridge cobalt centers, owing to the encapsulation of the central Co within the cluster core, the observed results support the contention that the $Co(OH_2)_6^{3+/2+}$ self-exchange electron transfer occurs by an inner-sphere mechanism via a bridging water versus the involvement of high-spin excited states of cobalt ion.

ASSOCIATED CONTENT

Supporting Information

Experimental details; table of crystal and refinement details and the crystallographic information file (CIF) for co-crystallized **1** and **2**; ^1H and ^{19}F NMR spectra, ESI-MS spectra, cyclic voltammograms, visible and NIR spectra; mid-IR and far-IR spectra, and the details of the self-exchange rate constant calculations. This material is available free of charge via the Internet at http://pubs.acs.org.

AUTHOR INFORMATION

Corresponding Author

dnocera@fas.harvard.edu

Notes

The authors declare no competing financial interest.

ACKNOWLEDGMENTS

We thank Dr. Thomas Teets and Prof. Yogesh Surendranath for many productive discussions, Prof. Danna Freedman for discussions and assistance collecting magnetic data, and Jeffrey Simpson for useful and time-saving suggestions for acquiring and processing NMR data. This research was supported by AFOSR FA9550-13-1-0028.

REFERENCES

(1) Kanan, M. W.; Nocera, D. G. *Science* **2008**, *321*, 1072−1075.
(2) Surendranath, Y.; Dincă, M.; Nocera, D. G. *J. Am. Chem. Soc.* **2009**, *131*, 2615−2620.
(3) Kanan, M. W.; Surendranath, Y.; Nocera, D. G. *Chem. Soc. Rev.* **2009**, *38*, 109−114.
(4) Surendranath, Y.; Kanan, M. W.; Nocera, D. G. *J. Am. Chem. Soc.* **2010**, *132*, 16501−16509.
(5) Pijpers, J. J. H.; Winkler, M. T.; Surendranath, Y.; Buonassisi, T.; Nocera, D. G. *Proc. Natl. Acad. Sci. U.S.A.* **2011**, *108*, 10056−10061.
(6) Reece, S. Y.; Hamel, J. A.; Sung, K.; Jarvi, T. D.; Esswein, A. J.; Pijpers, J. J. H.; Nocera, D. G. *Science* **2011**, *334*, 645−648.
(7) Surendranath, Y.; Bediako, D. K.; Nocera, D. G. *Proc. Natl. Acad. Sci. U.S.A.* **2012**, *109*, 15617−15621.
(8) Cox, C. R.; Winkler, M. T.; Pijpers, J. J. H.; Buonassisi, T.; Nocera, D. G. *Energy Environ. Sci.* **2013**, *6*, 532−538.
(9) Nocera, D. G. *Acc. Chem. Res.* **2012**, *45*, 767−776.
(10) Zhong, D. K.; Gamelin, D. R. *J. Am. Chem. Soc.* **2010**, *132*, 4202−4207.
(11) Zhong, D. K.; Cornuz, M.; Sivula, K.; Grätzel, M.; Gamelin, D. R. *Energy Environ. Sci.* **2011**, *4*, 1757−1764.
(12) Steinmiller, E. M. P.; Choi, K.-S. *Proc. Natl. Acad. Sci. U.S.A.* **2009**, *106*, 20633−20636.
(13) McDonald, K. J.; Choi, K.-S. *Chem. Mater.* **2011**, *23*, 1686−1693.
(14) Seabold, J. A.; Choi, K.-S. *Chem. Mater.* **2011**, *23*, 1105−1112.
(15) Risch, M.; Khare, V.; Zaharieva, I.; Gerencser, L.; Chernev, P.; Dau, H. *J. Am. Chem. Soc.* **2009**, *131*, 6936−6937.
(16) Kanan, M. W.; Yano, J.; Surendranath, Y.; Dincă, M.; Yachandra, V. K.; Nocera, D. G. *J. Am. Chem. Soc.* **2010**, *132*, 13692−13701.
(17) Du, P.; Kokhan, O.; Chapman, K. W.; Chupas, P. J.; Tiede, D. M. *J. Am. Chem. Soc.* **2012**, *134*, 11096−11099.
(18) Farrow, C. L.; Bediako, D. K.; Surendranath, Y.; Nocera, D. G.; Billinge, S. J. L. *J. Am. Chem. Soc.* **2013**, *137*, 6403−6406.
(19) Lutterman, D. A.; Surendranath, Y.; Nocera, D. G. *J. Am. Chem. Soc.* **2009**, *131*, 3838−3839.
(20) Surendranath, Y.; Lutterman, D. A.; Liu, Y.; Nocera, D. G. *J. Am. Chem. Soc.* **2012**, *134*, 6326−6336.
(21) Habib, H. S.; Hunt, J. P. *J. Am. Chem. Soc.* **1966**, *88*, 1668−1671.
(22) Sutin, N.; Creutz, C. In *Inorganic Reaction and Methods*, Vol. *15*; Zuckerman, J. J., Ed.; Wiley-VCH: Weinheim, Germany, 1986; pp 16−49.
(23) Marcus, R. A.; Sutin, N. *Biochim. Biophys. Acta Rev. Bioenerg.* **1985**, *811*, 265−322.
(24) Macartney, D. H.; Sutin, N. *Inorg. Chem.* **1985**, *24*, 3403−3409.
(25) Endicott, J. F.; Durham, B.; Kumar, K. *Inorg. Chem.* **1982**, *21*, 2437−2444.
(26) Navon, G. *J. Phys. Chem.* **1981**, *85*, 3547−3549.
(27) Johnson, D. A.; Nelson, P. G. *Inorg. Chem.* **1999**, *38*, 4949−4955.
(28) Meally, S. T.; McDonald, C.; Karotsis, G.; Papaefstathiou, G. S.; Brechin, E. K.; Dunne, P. W.; McArdle, P.; Power, N. P.; Jones, L. F. *Dalton Trans.* **2010**, *39*, 4809−4816.
(29) Heintz, R. *Inorg. Synth.* **2002**, *33*, 74−82.
(30) Figgis, B. N.; Hitchman, M. A. *Ligand Field Theory and Its Applications*; Wiley−VCH: New York, 2000; p 209.
(31) Bain, G. A.; Berry, J. F. *J. Chem. Educ.* **2008**, *85*, 532−536.
(32) McKay, H. A. C. *Nature* **1938**, *142*, 997−998.
(33) Espenson, J. H. *Chemical Kinetics and Reaction Mechanisms*; McGraw-Hill: New York, 1981; Ch. 3−4.
(34) Sutin, N. *Annu. Rev. Nucl. Sci.* **1962**, *12*, 285−328.
(35) Zhou, Y. L.; Zeng, M. H.; Wei, L. Q.; Li, B. W.; Kurmoo, M. *Chem. Mater.* **2010**, *22*, 4295−4303.
(36) Richens, D. T. *Chem. Rev.* **2005**, *105*, 1961−2002.
(37) Izutsu, K. *Electrochemistry in Nonaqueous Solutions*; Wiley-VCH: Weinheim, 2002; Ch. 4.
(38) Meally, S. T.; McDonald, C.; Kealy, P.; Taylor, S. M.; Brechin, E. K.; Jones, L. F. *Dalton Trans.* **2012**, *41*, 5610−5616.
(39) Harris, D. C. *Quantitative Chemical Analysis*; W. H. Freeman: New York, 2003; Ch. 3.
(40) Evans, D. F. *J. Chem. Soc.* **1959**, 2003−2005.
(41) Sur, S. K. *J. Magn. Reson.* **1989**, *82*, 169−173.
(42) Murrie, M. *Chem. Soc. Rev.* **2010**, *39*, 1986−1995.

(43) Klaeui, W.; Eberspach, W.; Guetlich, P. *Inorg. Chem.* **1987**, *26*, 3977−3982.
(44) Sutin, N. *Acc. Chem. Res.* **1982**, *15*, 275−282.
(45) Brunschwig, B. S.; Creutz, C.; Macartney, D. H.; Sham, T.-K.; Sutin, N. *Faraday Discuss. Chem. Soc.* **1982**, *74*, 113−127.
(46) Brunschwig, B. S.; Logan, J.; Newton, M. D.; Sutin, N. *J. Am. Chem. Soc.* **1980**, *102*, 5798−5809.
(47) Marcus, Y. *Ion Solvation*; Wiley: New York, 1985; Ch. 6.
(48) Sutin, N. In *Progress in Inorganic Chemistry*; Lippard, S. J., Ed.; Wiley: New York, 1983; Vol. *30*, pp 441−499.
(49) Wright, M. R. *An Introduction to Aqueous Electrolyte Solutions*; Wiley: New York, 2007; Ch. 10.
(50) Nielson, R.; Wherland, S. *Inorg. Chem.* **1984**, *23*, 1338−1344.
(51) Braga, T. G.; Wahl, A. C. *J. Phys. Chem.* **1985**, *89*, 5822−5828.
(52) Beattie, J. K.; Best, S. P.; Skelton, B. W.; White, A. H. *J. Chem. Soc., Dalton Trans.* **1981**, 2105−2111.
(53) Cossee, P. *J. Inorg. Nucl. Chem.* **1958**, *8*, 483−488.
(54) Radaelli, P. G.; Cheong, S.-W. *Phys. Rev. B* **2002**, *66*, 094408.
(55) Křápek, V.; Novák, P.; Kuneš, J.; Novoselov, D.; Korotin, D. M.; Anisimov, V. I. *Phys. Rev. B* **2012**, *86*, 195104.
(56) Piotrowiak, P.; Miller, J. R. *J. Phys. Chem.* **1993**, *97*, 13052−13060.
(57) Coddington, J.; Wherland, S. *Inorg. Chem.* **1996**, *35*, 4023−4028.
(58) Marcus, R. A. *J. Phys. Chem. B* **1998**, *102*, 10071−10077.
(59) Savéant, J.-M. *J. Am. Chem. Soc.* **2008**, *130*, 4732−4741.

dx.doi.org/10.1021/ja404469y | *J. Am. Chem. Soc.* 2013, 135, 15053−15061